



Atomic scale foundation of temperature-dependent bonding constraints in network glasses and liquids

M. Bauchy, M. Micoulaut *

Laboratoire de Physique Théorique de la Matière Condensée, Université Pierre et Marie Curie, Boite 121, 4, place Jussieu 75252 Paris Cedex 05, France

ARTICLE INFO

Article history:

Received 17 September 2010

Received in revised form 21 February 2011

Available online 13 April 2011

Keywords:

Glasses;
Bond constraint theory;
Molecular simulations;
Silicates

ABSTRACT

The behaviour of bonding constraints with temperature is analyzed from an atomic scale approach (Molecular Dynamics, MD) combined with partial bond angle distributions (PBAD). The latter allows to have access to the second moments (standard deviations) of the distributions. Large (small) standard deviations correspond to large (small) angular excursions around a mean value, and are identified as broken (intact) bond-bending constraints. A similar procedure is used for bond-stretching constraints. Systems examined include glassy and liquid disilicate $2\text{SiO}_2\text{-Na}_2\text{O}$ (NS2). In the glass, MD constraint counting closely matches Maxwell enumeration of constraints using the octet binding (8-N) rule. Results show that the standard deviations of the partial bond angle distributions increase with temperature and suggest a softening of bond-bending constraints. A bimodal bonding oxygen distribution is obtained for $T > T_g$, and the fraction of thermally activated broken bond-bending constraints computed as a function of temperature. Overall, these results provide a microscopic rationale for extending constraint counting from chalcogenides to complex oxides, and also a numerical basis for recent functional forms of temperature-dependent constraints proposed from energy landscape approaches.

© 2011 Elsevier B.V. All rights reserved.

1. Introduction

Rigidity theory offers a practical computational scheme using topology, namely the constraint Maxwell counting procedure, to address several issues in contemporary investigations of non-crystalline solids [1–4]. It has led to the recognition of a rigidity transition [2] which separates flexible glasses, having internal degrees of freedom that allow for local deformations, from stressed rigid glasses which are “locked” by their high bond connectivity. Mathematically, this transition (also termed Phillips–Thorpe rigidity percolation) is reached when the number of bonding constraints (radial, stretching [BS] and angular, bending [BB]) per atom n_c equals the number of degrees of freedom, that is 3 in three dimensions. Applications on chalcogenide network formers such as Ge–Se [5], binary oxides ($\text{GeO}_2\text{-Na}_2\text{O}$, [6]) or multicomponent glasses (Ge–P–Se, [7]) have shown that a certain number of physical and chemical properties display a threshold behaviour or a change in régime when passing through the transition [8], so that rigidity theory provides a basic framework to analyze in depth compositional trends in physical properties of network glasses. More recently, one has found that the onset of rigidity takes place over a finite compositional interval [9], corresponding to an intermediate phase (IP) with some remarkable properties such as absence of network stress and ageing, space-filling

tendency, non-linear ionic conduction, and maximal configurational entropy S_c [10]. Concerning the latter, as S_c is found to be proportional to the inverse of the activation energy E_A for viscous flow [11], one also expects to have E_A minimum found to be the minimum in the IP, or a strong behaviour for the corresponding glass-forming liquid, which is indeed observed experimentally for selected systems [12]. On the other hand, it has been shown that the primary contribution to S_c is through floppy modes [13] which only exist in the flexible phase and, to some extent, in the IP. The nature of the IP and a link with the configurational entropy (and eventually the entropy of mixing) is still under consideration.

Enumeration of bonding constraints works well in fully connected networks at $T = 0$ K. In practice, this situation is fulfilled as long as the viscosity (i.e. the bonding fraction) of the system is very high, typically at $T < T_g$. Extension of constraint theory to the liquid phase poses new scientific challenges but with new rewards: it can lead to an increased understanding of oxide and chalcogenide glass-forming liquids. Such an extension would permit investigating how far liquid properties can be described in terms of the topology/rigidity of the underlying low-temperature network structure.

Recently, it has been shown from neutron spin-echo spectroscopy that the rigidity concept could be extended from the glass to the liquid [14]. The parameters giving the temperature dependence of the relaxation patterns of binary chalcogen melts have indeed shown to be linearly dependent on the low temperature mean coordination number \bar{r} , the central quantity in rigidity theory. Relaxational phenomena in Ge–Se using the constraint approach have been also

* Corresponding author.

E-mail address: mmi@lptl.jussieu.fr (M. Micoulaut).

reported from liquid-state NMR [15]. In parallel, new ideas have been brought into rigidity theory by Mauro et al., using an energy landscape approach [16]. These ideas permit to describe accurately the fragility and glass transition temperature in different binary liquids [17,18], based on a construction that uses a function $q(T)$ encoding the temperature behaviour of bonding constraints via $n_c(T) = q(T)n_c(T=0)$. It leads to the function $q(T)$ with the property,

$$\lim_{T \rightarrow 0} q(T) = 1 \quad \lim_{T \rightarrow \infty} q(T) = 0 \quad (1)$$

Other applications have, since then, been reported [19,20]. In fact, in the limit of zero temperature, there is no thermal energy that can be used to overcome the energy associated with a constraint. It corresponds to the usual situation where constraint counting algorithms can be applied with confidence. At a finite temperature however, a fraction of these constraints are broken by thermal activation. Nevertheless, one may expect that the low temperature behaviour $q(T) \approx 1$ holds as long as the system is in the glassy state. In the other limit corresponding to the high temperature liquid, all constraints must be broken so that they do not contribute to the rigidity of the system and $q(\infty) \approx 0$. A simple expression fulfilling the aforementioned limits and introduced in Ref. [16] is:

$$q(T) = \left[1 - \exp\left(-\frac{\Delta F^*}{k_B T}\right) \right]^{\nu t_{obs}} \quad (2)$$

where ΔF^* is the activation energy needed to break a constraint, ν is the associated vibrational attempt frequency and t_{obs} is the observation time. Assuming that νt_{obs} is large, $q(T)$ can be approximated by a step function [16] with a reset temperature at which the constraints are considered as broken. Since BB are considered to be softer than BS interactions (e.g. 19 meV against 31 meV in Ge-As-Se [21]), a hierarchy of reset temperatures can be defined, depending on the atoms and the nature of the chemical bonding associated with a constraint.

The aim of this paper is to derive a physical basis for Eq. (2) and, more generally, to provide an atomic scale picture that could account for the behaviour of the number of rigid constraints with temperature, using Molecular Dynamics (MD). Our results are obtained for the $2\text{SiO}_2\text{-Na}_2\text{O}$ system (NS2) which represents a base material for various multicomponent systems found in Earth Sciences and glass industry. The choice of a silicate system is also motivated by the fact that a direct constraint counting following the “8-N” (or octet) rule [22] leads to results for the rigidity transition location which are consistent with experimental observation [6,23]. Here N represents the outer shell electrons, and this rule works well for directional covalent bonds. However, it is well known that the coordination number of certain species do not follow this rule. For instance, sodium interacts mostly through electrostatic non-directional forces, making the application of a rule proposed for directional covalent bonds unlikely. This departure from the 8-N rule manifests in binary oxides, and it has been found that sodium has between four and six neighbours [24–27]. In silicate glasses, a variety of coordination numbers have been found for the alkali and alkaline earth cations [28–30], although the underlying bond distances are not equivalent [28,31].

Our results are consistent with the findings on structure and coordination numbers reported for silicates [32], but they also show that in the glassy state the enumeration of relevant bonding constraints very closely follows what would be obtained from the 8-N rule [23]. An analysis of partial bond angle distributions derived from Molecular Dynamics (MD) trajectories in the glassy state, provides a framework to evaluate bending constraints with temperature that can be used to describe the liquid state. The present results support the aforementioned phenomenological Mauro model [16], and provide a numerical estimate of the involved parameters. As the

construction is rather general, we believe that the method can be applied for any system studied by Molecular Simulations. It, therefore, opens the perspective to study glass-forming liquids using topological tools resulting from a combination of MD and constraint theory. On the NS2 system, it would be beyond the scope of the present work to give a complete description of its physical and chemical properties. We refer the reader to a certain number of relevant topical reviews [33–35].

2. Results

To obtain the results presented in this work, we have simulated in a (N,V,T) Ensemble a 3000 atomic system of a $2\text{SiO}_2\text{-Na}_2\text{O}$ (NS2) glass using a two-body potential initially introduced by Teter [36] and extensively used for structural and dynamics studies in sodium silicates [37,38]. The size of the simulation cell has been fixed to recover the experimental density [39] of the glass (2.37 g/cm^3). The equations of motion have been integrated using a leap-frog Verlet algorithm with a time-step of 2 fs. Starting from an initial temperature of 5000 K, we have selected a certain number of temperatures in steps of 500 K in the liquid state, and obtained a glass after a quench at a cooling rate of 1 K/ps. The resulting numerical T_g determined from the slope break between the low and the high temperature behaviour of the total energy $E(T)$ is found to be of about 2120 K. Averages have been performed over $10^4 - 10^5$ steps on the final configuration. The resulting structure at 300 K is by all means comparable to the one obtained in [37,38]. Instead of analyzing the obtained structure in terms of Si-, O and Na-based correlations, we adopt here a slightly different framework and split the analysis performed on oxygen into contributions coming from bridging oxygens (BO, connecting two tetrahedra) and so-called non-bridging oxygen (NBO, non-bridging oxygen, found in the vicinity of a sodium atom), which are responsible for the depolymerization of the network.

Fig. 1 shows respectively Na-, NBO- and BO-centred pair distribution functions, yielding the relevant bond distances at the first peak position. We find $d_{\text{Si-O}} = 1.61 \text{ \AA}$ (observable from the first sharp peak in the BO and NBO-centred pair distribution functions of Fig. 1), $d_{\text{O-O}} = 2.62 \text{ \AA}$, $d_{\text{Si-Si}} = 3.15 \text{ \AA}$ and $d_{\text{Na-O}} = 2.38 \text{ \AA}$ (first peak in the Na-centred pair distribution function) which compare favorably to experimental results, as it has been found from neutron diffraction [40,41] (respectively EXAFS) $d_{\text{Si-O}} = 1.622 \text{ \AA}$ (respectively 1.668 \AA [42]), $d_{\text{O-O}} = 2.626 \text{ \AA}$, and $d_{\text{Na-O}} = 2.36 \text{ \AA}$ (respectively 2.30 \AA for a NS4 glass [43]). The first peak in NBO and BO pdfs is found at a distance of 1.555 \AA and 1.605 \AA respectively. Such a difference in bond length is found in the corresponding crystalline $\alpha\text{-Na}_2\text{Si}_2\text{O}_5$ for which it is found $d_{\text{BO-NBO}} = 0.06 \text{ \AA}$ [44], while quantum orbital calculations lead to $d_{\text{BO-NBO}} = 0.1 \text{ \AA}$ [45]. A detailed discussion on model accuracy can be found in Ref. [38].

The secondary peak at 2.615 \AA in the NBO-centred pdf contains a shoulder which is identified with the NBO-Na distance at 2.36 \AA , also seen from the principal peak in the Na pdf. The main contribution to this secondary NBO peak comes from NBO-BO correlations, as also detected from the corresponding peak in the BO-centred pdf. With increasing temperature (from 300 K to 2000 K, red curve in Fig. 1), the peaks broaden or even vanish as seen from the Na-centred pdf. Angles and bond angle distributions (BAD) are discussed below.

2.1. MD method of constraint counting

In rigidity of macroscopic structures, tensile forces are enumerated on bar networks or trusses [46]. In atomic scale networks, relevant forces between atoms have to be identified, and these include bond-stretching (BS) and bond-bending (BB) forces. As in classical mechanics however, instead of treating forces and querying about motion, one may follow the opposite direction and try to relate atomic motion to the absence of a restoring force which maintains bonds and

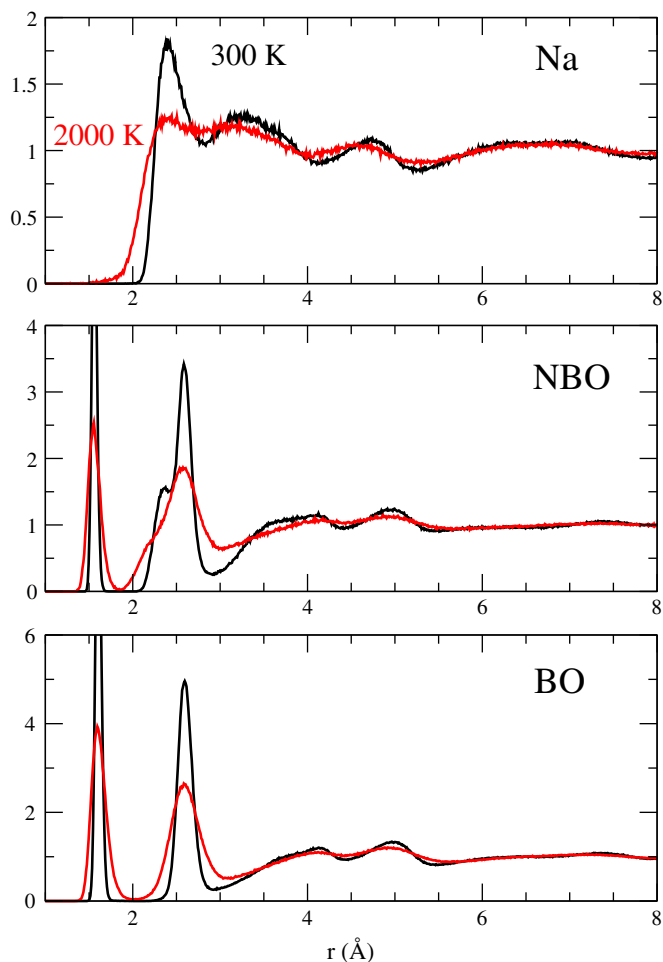


Fig. 1. Na-, NBO- and BO-centred pair distribution functions of a NS2 glass at 300 K (black) and 2000 K (red).

angles fixed at a value around a mean value (Fig. 2). This is the starting consideration of the present approach derived from Molecular Dynamics. Having generated the atomic scale configurations at different temperatures from MD, we now apply a structural analysis in relation to rigidity theory as follows. The coordination number (or number of neighbours) r_i , hence the number of BS constraints (equal to $r_i/2$), can be calculated by integrating first the pair distribution function up to its first minimum. We find $r_{Si} = 4$, $r_{BO} = 2$, $r_{NBO} = 1$, and $r_{Na} = 5$ (Fig. 3a), as in other simulations [37,38] and experiments [41]. An alternative means [47] for getting the coordination numbers is to

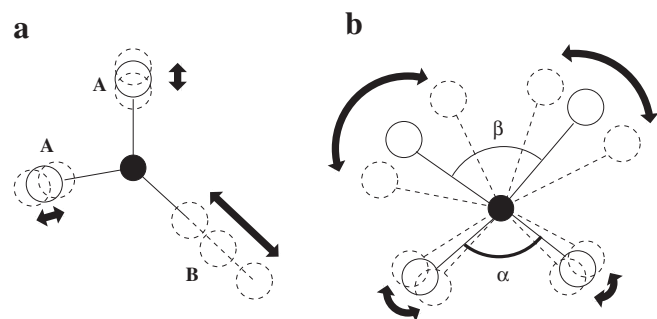


Fig. 2. Method of constraint counting from MD-generated configurations. Large (small) radial (a) or angular (b) excursions around a mean value are characterized by large (small) standard deviations on bond B or angle β (small on A or α), representing broken (intact) constraints.

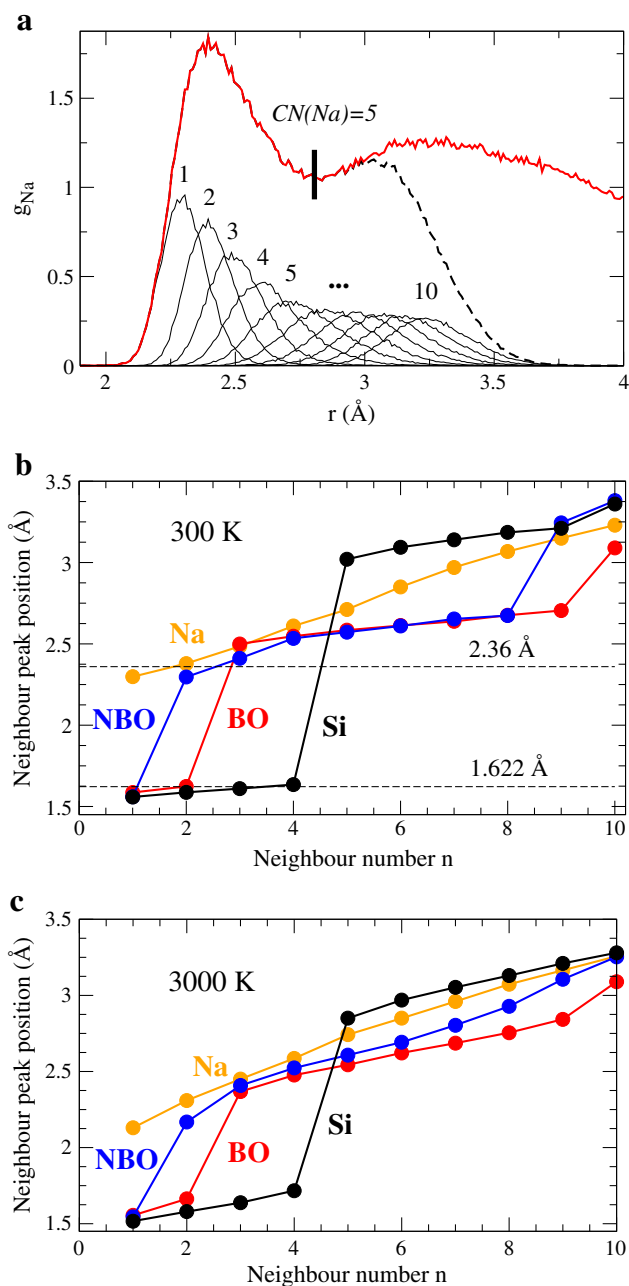


Fig. 3. a) Na pair distribution function g_{Na} (pdf, red curve, same as Fig. 1) and its decomposition into 10 neighbour distributions out of which are computed corresponding radial standard deviations σ_r . The broken curve is the sum of the 10 distributions. b) Position of the neighbour distribution peaks at 300 K for Si, Na, NBO and BO atoms as a function of neighbour number n . The horizontal broken lines at 2.36 Å and 1.622 Å correspond respectively to the experimental Na–O and Si–O distances [40,41]. c) Same quantities as in b) but now at 3000 K.

represent the decomposition into neighbour distributions (black curves in Fig. 3a). The position of these distributions is shown in Fig. 3b and c (i.e. neighbour peak positions (in Å) as a function of the neighbour number n (from 1 to 10)). A clear jump is obtained between the first and the second shell of neighbours, and reproduces what is obtained from a usual direct integration of the pdfs: the coordination number r found at the minimum of the pdf corresponds to the r^{th} neighbour distribution. Noteworthy is the fact that the neighbour shells of sodium are not very well defined as the positions are found to smoothly increase with neighbour number, in contrast with e.g. the behaviour found for silicon. The single NBO neighbour found at $n = 1$ is a silicon atom which give rise to the peak found at

1.61 Å in the NBO pdf (Fig. 3b), whereas the second neighbour coincides, indeed, with the first sodium neighbour found at 2.36 Å (Fig. 1). The peak broadening obtained at higher temperatures (e.g. 2000 K in Fig. 1) leads to a global settling of the distributions corresponding to the second shell of neighbours although first and second shells can still be well separated (see. also Fig. 5).

The splitting of the pdfs into neighbour distributions (such as Fig. 3a) and the focus on their corresponding standard deviations σ_r give an estimate of the strength of the interaction that is needed to maintain a bond distance (a stretching constraint) of a given neighbour fixed (see also Fig. 2). In other words, large σ_r 's will be associated with soft interactions and to an increased spatial extent for the bond length, whose corresponding constraint can be considered as ineffective (i.e. broken).

We remind the reader that the statistical averages are performed over time (trajectories) and space (simulation box) so that the computed σ_r represent a global estimate for the sample, regardless of any possible time or spatial fluctuations of standard deviations and constraints that may exist. This choice is motivated by the fact that our goal is to connect the MD simulation to the global (or Maxwell) constraint counting procedure only. We keep in mind, however, that alternative statistical mechanics averages may be used [48,49] to study self-organized rigidity and the intermediate phase [50,51].

As already mentioned, it is found (Fig. 3a) that the number of sodium neighbours is five, computed at the minimum of the Na-centred pdf found at 2.75 Å, a minimum which coincides with the location of the fifth neighbour distribution. However, the computation of the second moments (standard deviations), σ_r , for the neighbour distributions shows that these Na-based distributions have σ_r 's that are substantially higher (0.1 Å, Fig. 4) than those obtained for the other atoms (NBO, BO, Si, all about 0.025 Å).

Concerning the NBO atoms, one can split the decomposition of neighbour distributions, seen at a global level in Fig. 4, into contributions coming from Na (NBO-Na) and from Si atoms (NBO-Si) (blue curve, Fig. 5). It is seen that the radial excursion σ_r of the first NBO-Si bond found at 1.55 Å is very similar to the one obtained for the BO-Si at 1.605 Å, with $\sigma_r \approx 0.03$ Å. It contrasts with the value of σ_r found for the first NBO-Na bond at a somewhat higher value ($\sigma_r = 0.09$ Å). The latter is, however, still low as compared to the other contributions arising from the next shell of neighbours which are found to be at least equal to 0.15–0.20 Å.

In conclusion, one can stress that low radial standard deviations lead to intact bond-stretching constraints (\propto neighbours $\times \frac{1}{2}$). In the NS2 glass, three constraints are well-defined and arise from the first shell of neighbours: two for the silicon atom ($4 \times \frac{1}{2}$), one for the BO

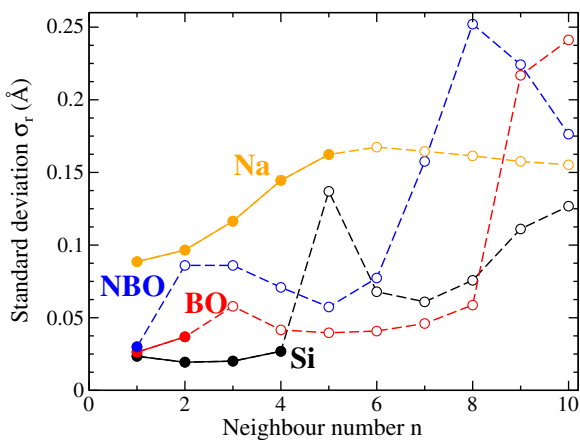


Fig. 4. a) Radial standard deviations σ_r at 300 K for Si, BO, NBO and Na centred neighbour distributions as a function of the neighbour number n . All neighbours are considered here. Open symbols and broken lines correspond to neighbours found at the second shell.

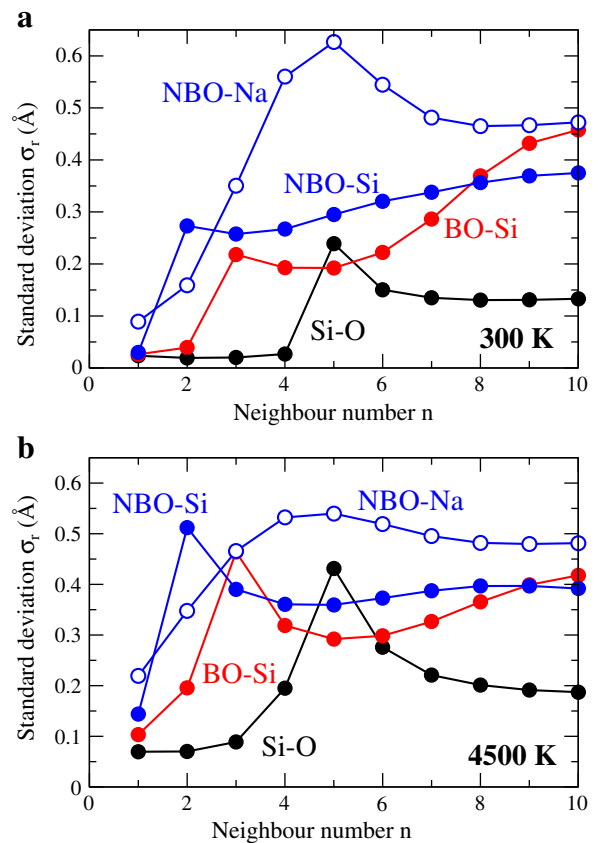


Fig. 5. a) Radial standard deviations σ_r at 300 K for selected pairs Si-O, BO-Si, NBO-Si and NBO-Na centred neighbour distributions as a function of the neighbour number. b) Same quantities as in a) at 4500 K.

atom ($2 \times \frac{1}{2}$). An additional constraint (coming from the NBO-Na interaction) can be considered ($1 \times \frac{1}{2}$), due to its low radial excursion, less than 0.1 Å.

2.2. Partial bond-angle distribution and bending constraints

The number of bond-bending constraints is determined from partial bond angle distributions (PBAD) $P(\theta)$ introduced recently [52,53]. For each type of a central atom 0, the N first neighbours are selected and the $N(N-1)/2$ corresponding angles $i\hat{0}j$ ($i=1..N-1$, $j=2..N$) such as $\hat{102}$, $\hat{103}$, $\hat{203}$, etc. (see top panel of Fig. 6) are calculated. The first moment of these PBADs gives access to the mean angle $\bar{\theta}$. Computation of the second moment σ_{θ}^2 , or standard deviation σ_{θ} , of a $P(\theta)$ distribution gives a quantitative estimate of the angular excursion around the mean value, thus providing a measure of the strength of the bond-bending restoring forces.

Fig. 6 shows such PBADs for central Si, Na and BO in a NS2 glass. As one can see, some angles display a very sharp distribution centred at the tetrahedral angle of 109° (e.g. angle 1:102 in the Si panel of Fig. 6), in agreement with the existence of sp^3 hybridization of the Si atom. Others PBAD arising from the second shell of neighbours (e.g. the fifth neighbour of a central Si atom) have a broad distribution which will be characterized by a large standard deviation σ_{θ} . Angles displaying a broad distribution are, again, identified with intrinsically broken constraints (this time, bond-bending) as there must be a weak interaction to maintain the angle fixed around its mean value $\bar{\theta}$.

We find that most of the sodium distributions are centred at $\approx 100^\circ$, in agreement with an alternative analysis splitting the Na-centred bond angle distributions into contributions coming either from BO or NBO atoms [38,54]. We are not aware of any published work on Na-centred BAD's. The BO-centred BAD (angle 102, Fig. 6b) is

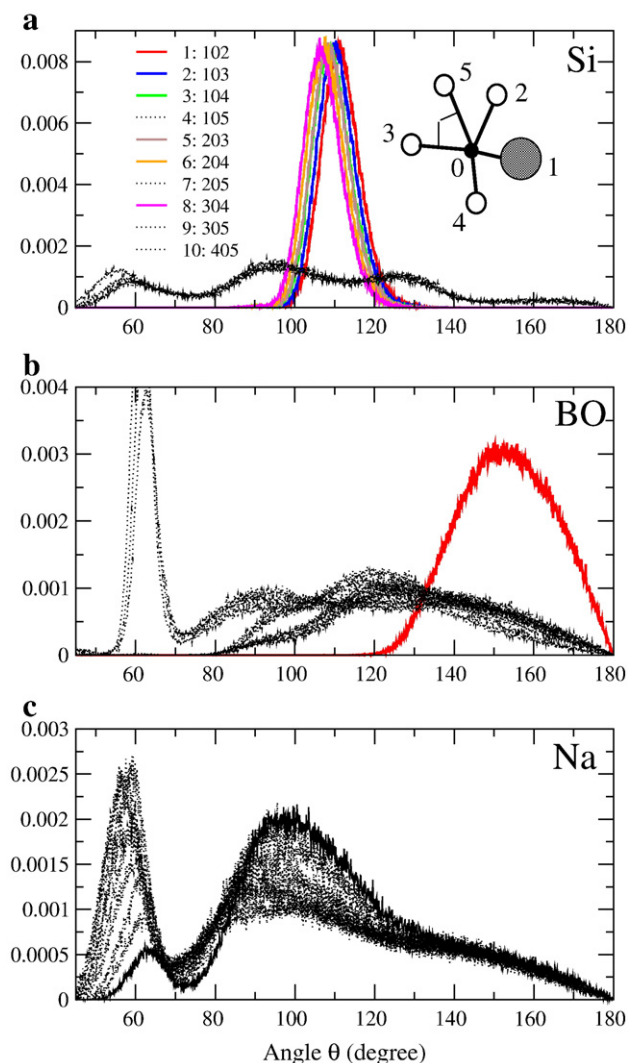


Fig. 6. Ten Si-, BO- and Na-centred partial bond angle distributions of a NS2 silicate glass for an arbitrary $N=5$. Note that one can distinguish between BO (bridging oxygens connecting two Si tetrahedra) and non-bridging oxygens (NBO, not represented), the latter being found in the vicinity of sodium atoms. The colored curves correspond to distributions having a standard deviation σ_θ lower than 18° (see also Fig. 7). Other distributions are represented by broken lines. The top (Si) panel shows a molecule used for the PBAD algorithm: from the selection of a central atom 0, and for a given number of neighbours (here $N=5$), one computes all possible bond angle distributions between sets of neighbours (e.g. the marked 305).

found to be centred at 150° , in agreement with previous MD simulations [38], although this quantity has been found to be highly sensitive to the interaction potential [55] when compared to experiments [42].

Fig. 7 represents the standard deviations σ_θ of the Si-, BO-, NBO- and Na-centred PBADs as a function of an arbitrary angle number (see also the definition of the angle labelling in the inset of Fig. 6a). These quantities have been computed from the PBADs represented in Fig. 6. One finds that only a limited number of distributions have a low standard deviation σ_θ : the six Si-centred angles defining the tetrahedron, leading to five independent constraints, and one BO bond angle. Contributions from NBO and Na have larger standard deviations, with $\sigma_\theta > 25^\circ$, and we consider their contributions to network rigidity to be ineffective. Thus, the present results on angles are found to match exactly a Maxwell count assuming the 8-N rule, including the assumption of a broken BB constraint for the NBO atom [56] because of the increased angular motion that manifests from the non-directional ionic Na-NBO interaction.

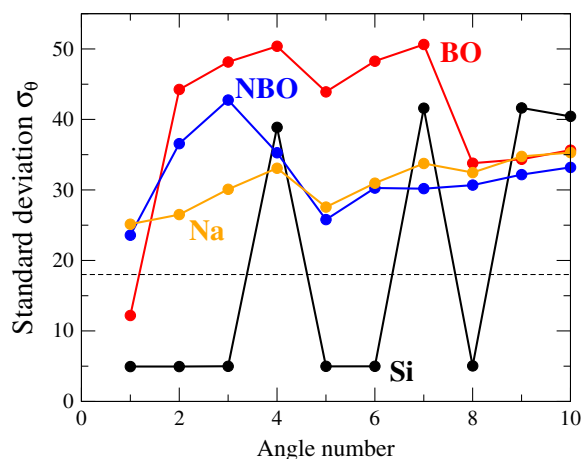


Fig. 7. Standard deviations σ_θ of Si-, BO-, Na- and NBO-centred partial bond angle distributions as a function of the angle number. The broken horizontal line represents an approximate limit between intact and broken angular constraints.

2.3. Consequences

In Table 1, we summarize the count of constraints in sodium silicate glasses $(1-x)\text{SiO}_2-x\text{Na}_2\text{O}$. One finds a rigid to flexible transition [2] in these silicates at the concentration of $x_c=20\%$ Na_2O , where furthermore optimal glass formation is expected, according to the Phillips stability criterion [1]. There is a large body of experimental evidence which supports the existence of such a transition.

The ease of vitrification in glasses can be tracked either from the crystallisation rate or from the vitrification enthalpy. Fang et al. [57] have reported such studies for alkali silicates, based on a measure of the critical cooling rates to avoid crystallization, using the so-called temperature-time-transformation (TTT) studies [58]. Their results show a minimum in the critical cooling rate, q_c , near 20% Na_2O composition; the correlation between q_c and x_c can be extended with confidence to potassium silicates [59]. Note that such correlations have also been reported for the $\text{Ge}_x\text{Se}_{1-x}$ binary in which slow cooling allows glass formation only at compositions that are close to the rigidity transition composition [60].

Glass forming tendency is also found to increase for systems that are able to increase their melt viscosity down to lower temperatures [61], for instance at eutectic compositions because such freezing-point depressions bring the system to lower temperatures and higher viscosities. For sodium and potassium silicates, the location of the composition of the minimum of the critical cooling rate is found to correlate well with the viscosity maximum [62] and with the rigid to flexible threshold composition x_c , a feature also reported for alkali tellurates [63].

Finally, and most importantly, it has been observed that an elastic energy providing a measure of the number of floppy modes, is found to be zero in the stressed rigid phase at $x < 20\%$. Once the system becomes flexible for $x > x_c$ [23], this energy becomes non-zero. The corresponding floppy mode energy has been computed to be 0.12 meV [59]. In parallel, a minimum in the non-reversing heat flow at the glass transition has been detected from modulated differential scanning

Table 1

Bond-stretching and bond-bending constraint counting in sodium silicate glasses, total number of constraints n_c , and the location of the optimally constrained network composition x_c . The composition $(1-x)\text{SiO}_2-x\text{Na}_2\text{O}$ has been rewritten under the form: $\text{Si}_{1-x}\text{BO}_{2-3x}\text{Na}_{2x}\text{NBO}_{2x}$.

Si^{BS}	Si^{BB}	BO^{BS}	BO^{BB}	NBO^{BS}	NBO^{BB}	Na^{BS}	Na^{BB}	n_c	x_c
$2(1-x)$	$5(1-x)$	$2-3x$	$2-3x$	$2x$	-	x	-	$11-10x$	0.2

calorimetry, similar to results found in chalcogenide network glasses [64,65].

3. Constraints in the liquid phase

We now turn to the liquid state ($T > T_g$) by following the analysis performed in the glass at increasing temperatures. Specifically, we focus on the radial and angular standard deviations computed from neighbour and partial bond angle distributions. As $T > T_g$, bond lifetimes decrease [66], and diffusion onsets on computer timescales. We find $D_{Na} = 3.1 \times 10^{-5} \text{ cm}^2 \text{ s}^{-1}$ at 1500 K (and $D_{Na} = 4.15 \times 10^{-5} \text{ cm}^2 \text{ s}^{-1}$ for the same temperature at zero pressure), which show a fair agreement with the experimental value measured at 1600 K [$D_{Na} = 6 \times 10^{-5} \text{ cm}^2 \text{ s}^{-1}$ [67]], but contrasts with a value obtained from another MD potential ($0.8 \times 10^{-5} \text{ cm}^2 \text{ s}^{-1}$ at 1900 K, [66]).

3.1. Stretching constraints

As seen earlier in Fig. 5, bonds having an intact stretching constraint at 300 K (a low standard deviation σ_r) will soften as temperature increases. While the three first oxygen neighbours of a silicon atom show only a mild change with T (from 0.02 Å to 0.06–0.08 Å), the radial excursion of the fourth atom increases substantially to nearly 0.2 Å at 4500 K (Fig. 8b). The latter figure tracks the behaviour of the radial

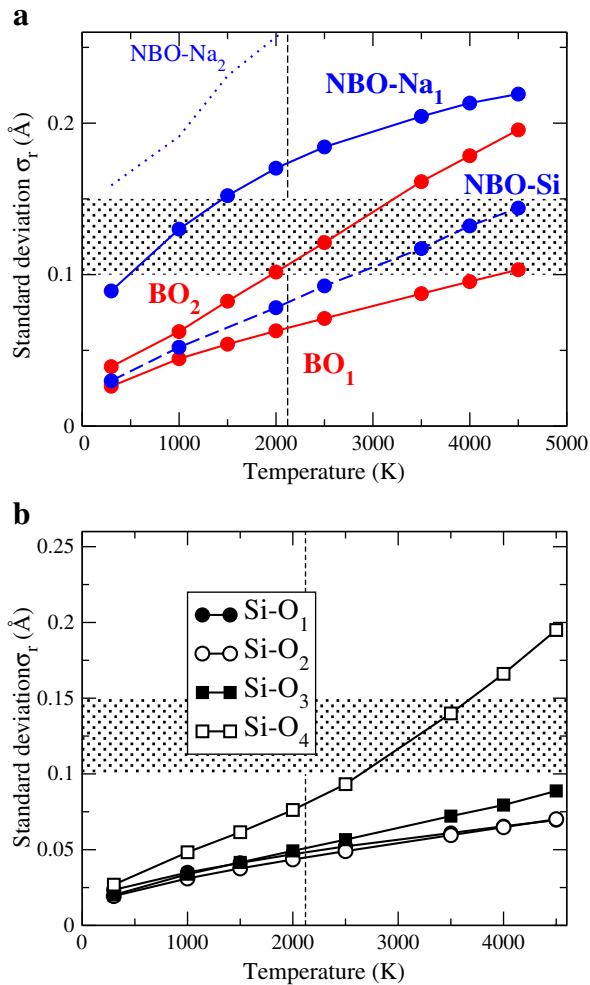


Fig. 8. Radial standard deviations σ_r for first neighbour distances of BO (BO₁ and BO₂) and first neighbour distances of NBO atoms (NBO-Si, NBO-Na₁ and NBO-Na₂) as a function of temperature. b) Same for the first four neighbour distances of Si. The shaded area indicates the region where constraints should become broken, on the basis of Fig. 5a. The broken vertical line is the computed numerical T_g . See text for details.

standard deviations σ_r of low temperature rigid constraints with respect to temperature. For the BO- and NBO-based standard deviations, the increase of σ_r is found to be more pronounced as compared to silicon, with σ_r growing from 0.095 Å to 0.225 Å at 4500 K. No abrupt change is found close to the glass transition.

Can a limit between a “broken” (or ineffective) and an “intact” constraint be defined on a firm basis? From Fig. 5a displaying the radial standard deviations, σ_r , at 300 K, we note that intact constraints arise from strong Si–O bonds having a low standard deviation of about 0.02 Å, while weaker ionic NBO–Na bonds exhibiting a gap between the first standard deviation (0.09 Å) and the second one (0.16 Å) constitute broken constraints. On this basis, the shaded area in Fig. 8 defines approximatively the range of σ_r where rigid constraints become ineffective as the temperature is increased. Thus the weakest bonds such as NBO–Na₁ (first Na neighbour of a NBO) and to a lesser extent BO₂ (corresponding to the neighbour number $n=2$) (Fig. 8), have their bond-stretching constraints broken before the glass reaches its transition temperature upon increasing T , the former around $T \approx 1000\text{K}$, the latter at $T \approx T_g$. Such a behaviour is not found for all other bonds in the system. At higher temperatures, all bonds have a standard deviation that is larger than $\sigma_r = 0.1$ Å, indicative of broken constraints. The silicon stretching constraints are found to be less sensitive to temperature increase, and only one constraint is considered broken at $T > T_g$ (Fig. 8b).

The present results agrees with the view described by Mauro and co-workers [16–18] who propose that at least one of the constraint onset temperatures T_i must fall above T_g , as the glass transition cannot occur unless one constraint is already rigid in the corresponding temperature range. From our results, it is shown that Na fulfills this requirement, as does partly the BO stretching constraints.

3.2. Bending constraints

We noted earlier (Fig. 7) that at low temperatures, NBO and Na angular distributions have standard deviations which are considerably larger ($\sigma_\theta > 20^\circ$) than BO and Si ones. The former are separated by a gap of about 10° with respect to the latter ones. In this respect, the feature appears to be similar to what has been found for radial standard deviations (Fig. 5a). To gain deeper insights into what constraints are relevant (low σ , intact) from those which are irrelevant (large σ , broken), we focus on the distributions of the standard deviations and their evolution with temperature across the glass transition. We track a given angle having a low σ_θ at 300 K (e.g. the BO angle 102 corresponding to Si–BO–Si) individually during the length of the simulation at a given temperature. Each angle of each BO has a certain angular distribution $P(\theta)$ and thus a unique standard deviation σ_θ . Considering the whole set of BO atoms leads to a distribution of standard deviations σ_θ that is followed with temperature.

Fig. 9 shows such distributions for temperatures in the 300 K $< T < 4500$ K range. At $T = 4500$ K, where all rigid constraints are broken because of thermal activation, we obtain a broad distribution of standard deviations with a mean centred near $\sigma_\theta 20\text{--}25^\circ$. At $T = 300$ K, the standard deviation is characterized by a rather sharp distribution centred at a low value for σ_θ (6°). Interestingly, when the glass approaches T_g (2120 K), the angular excursions increase from their low temperature value, and display a bimodal distribution located at a higher σ_θ . One distribution corresponds to broken constraints (Fig. 9), and, in fact, it grows with increasing temperature. The second distribution (narrow) arising from the low temperature system corresponds to intact constraints, and it progressively disappears. A broken line in Fig. 9 is drawn at the minimum of the bimodal distribution, which represents the “approximate limit in σ_θ separating intact from broken angular constraints.

It should be noted that we observe this feature not only for the BO angle (i.e. 102) but also for the Si angle distributions. As we noted

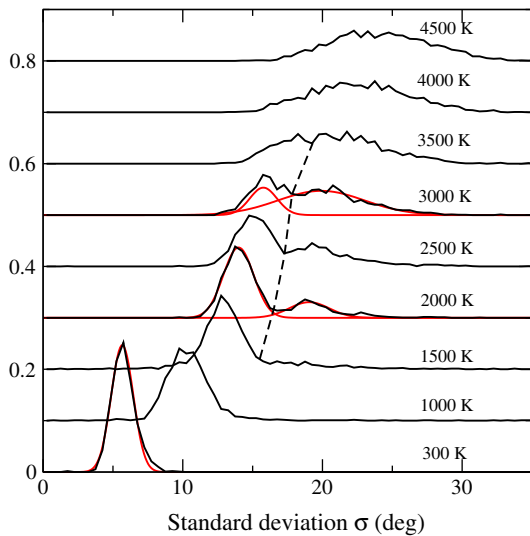


Fig. 9. Behaviour of the BO centred standard deviation distributions σ_θ for various temperatures of a NS2 glass. Note the bimodal distribution occurring at $T \approx 2000$ K. The broken line defines a boundary between broken and intact constraints, estimated to be about $\sigma_\theta = 15^\circ$ at low temperature. Gaussian fits (red curves) are shown for selected temperatures.

earlier, the fourth oxygen neighbour has its bond-stretching constraint broken (Fig. 8b) at high temperatures. One can see that the distribution of standard deviations associated with the latter departs from the other distributions once the temperature becomes larger than T_g . On an average, results (Fig. 10) for the silicon atoms (i.e. taking into account all four neighbours) display only a mild increase of the mean standard deviation $\bar{\sigma}_\theta$ from 5 to 15° (insert of Fig. 11). Finally, the general tendency for all angular standard deviations is the increase of their mean $\bar{\sigma}_\theta$ and their corresponding standard deviation σ_σ (inserts of Fig. 11).

3.3. Parameters for the Mauro–Gupta model

For certain distributions, a double Gaussian fit of the σ_θ distributions (red curves on Fig. 9) permits one to compute the fraction $q(T)$ of bond-bending constraints that are intact (Fig. 11). This

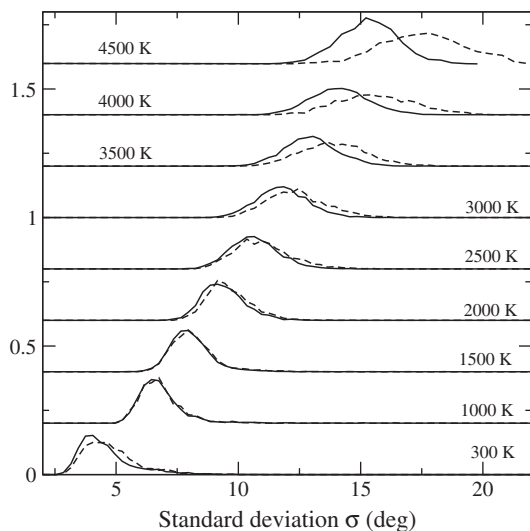


Fig. 10. Behaviour of the Si-centred standard deviation distributions σ_θ for various temperatures of a NS2 glass. The solid line correspond to angles 102, 103, and 203 and the broken line to angles 104, 204, and 304.

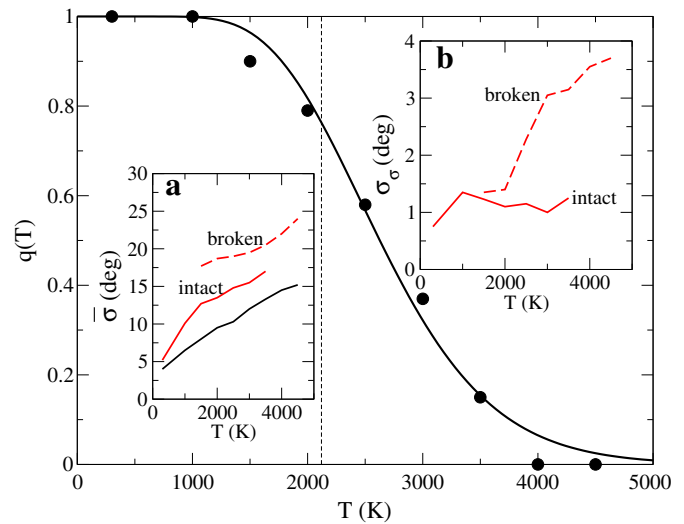


Fig. 11. Fraction $q(T)$ of intact BO constraints as a function of temperature. The solid curve is a fit using Eq. (2). Broken line is the computed glass transition temperature. The inserts a and b show respectively the mean standard deviation $\bar{\sigma}$ and the standard deviation σ_σ , computed from the bimodal distribution shown in Fig. 9. Red curves: BO angle 102 (Broken line: broken constraints, solid line: intact constraints). Black curve: Si angle 102.

is the case for the function q_{BO}^{BB} describing the fraction of bond-bending constraints of the BO atoms that are intact. A fit to our results using Eq. (2) leads to $\Delta F^* = 0.89$ eV and $\nu_{obs} = 34.3$, and an onset temperature (here the inflexion point of the fitted curve) equal to 2460 K, found somewhat greater than the simulated T_g (Table 2). The value for ΔF^* is the barrier needed for a BO atom to break a constraint. It can be compared with the activation energy $E_A = 1.7$ eV for viscosity/structural relaxation measured in the NS2 liquid [68] and with the one (2.26 eV) determined in a NS2 glass from the temperature behaviour of the oxygen diffusion constant using MD simulations [66]. The difference between E_A and our determined ΔF^* corresponds to the strain energy needed to locally deform the liquid structure and allow for oxygen diffusion.

For the Si function $q(T)$, we propose that $q_{Si}^{BB}(T)$ simply decreases from 5 to 3 at the onset temperature close to the T_g . This amounts to having one bond lost and 2 associated BB constraints lost. This happens over the temperature interval 2500–3000 K.

Finally, we stress that the present results should be rescaled with respect to a true glass transition temperature. It is well known that the very high quenching rates (here 1 K/ps) lead to glass transition temperatures that are much higher than those reported experimentally. For an NS2 glass, it is found indeed $T_g = 758$ K [23]. Rescaling the obtained onset temperatures (Table 2) using the latter gives an estimation of some “true” temperatures (rescaled temperatures T_{resc}) at which constraints can be considered as broken by thermal activation. For instance, it is found that for $T > 360$ K, all Na stretching

Table 2

Characteristic onset temperatures (in kiloKelvin) for the simplified Mauro–Gupta model in sodium silicate glasses, computed from the behaviour of the standard deviation with temperature.

	Si–O _{1–3} ^{BS}	Si–O _{1–3} ^{BB}	Si–O ₄ ^{BS}	Si–O ₄ ^{BB}	BO ^{BS}	BO ^{BB}	NBO ^{BS}	Na ^{BS}
T (kK)	–	–	3 ^a	T_g	2.5,4.0	2.46	3.8	1.0
T/T _g	–	–	1.42	1	1.18,1.89	1.16	1.79	0.47
T _{resc} (kK)	–	–	1.08	0.76	0.89,1.43	0.88	1.36	0.36

^a For the stretching constraints, the temperatures have been determined from the standard deviation behaviour with temperature of Fig. 8 and their centroid with respect to the shaded region.

constraints should be ineffective, and also contribute to an increased ionic conduction [69].

4. Summary and conclusions

In this article, we have applied a recently introduced method [52,53] which allows to compute accurately bonding constraints used in rigidity theory from Molecular Dynamics simulations to examine in detail the sodium silicate NS2. The central quantities of interest include radial and angular standard deviation of local distributions focusing either on neighbours or on partial angles. This allows to compute the respective number of bond-stretching and bond-bending constraints. In the silicate glass, we have found that the enumeration of constraints closely follows the 8-N bonding (octet) rule. The result provides excellent agreement with the observed rigid to flexible transition near 20% soda in sodium silicates. Our investigation of the liquid state leads to the identification of thermally activated broken constraints, mostly located on the Si-BO-Si angle, whose flexibility onsets close to T_g , and leads to a neat numerical evaluation of the fraction $q(T)$ of broken constraints. Silicon angular constraints are by far the strongest ones because of sp^3 hybridization of the orbitals. We find that only one stretching constraint is broken at high temperature, identified with the fourth neighbour distance, which also leads to an increased angular excursion.

There is a dichotomy between an “intact” and a “broken” constraint however. Although the strength of a BS force is about 3 times larger than a BB one [21], one clearly has weak Na–O and strong Si–O bonds in a sodium silicate network, even though each force qualifies as a constraint at the same level. This situation with hierarchical forces is well known in mechanical trusses, as both bars and springs with a variable spring constant need to be considered when a Maxwell stability criterion is searched.

We believe that our results open new interesting perspectives to study more challenging systems and/or systems undergoing structural changes which are not driven by composition but by pressure. For the former, because of a lack of information on the local structures and on the relevant motions that serve to qualify stretching and bending interactions, rigidity theory has been always inefficient. For the latter, until recently [17], subtle changes in structure induced by e.g. pressure or temperature have been difficult to describe from bonding constraints.

It is a pleasure to acknowledge many stimulating discussions with C. Bichara, P. Boolchand, M. Malki, J.C. Mauro, C. Massobrio, G.G. Naumis, J.C. Phillips, J.-Y. Raty, P. Simon. This work is supported by Agence Nationale de la Recherche (ANR) n.09-BLAN-0190-01.

References

- [1] J.C. Phillips, *J. NonCryst. Solids* 34 (1979) 155.
- [2] M.F. Thorpe, *J. NonCryst. Solids* 55 (1983).
- [3] D. Selvanathan, W.J. Bresser, P. Boolchand, *Phys. Rev. B* 61 (2000) 15061.
- [4] M. Micoulaut, J.C. Phillips, *Phys. Rev. B* 67 (2003) 104204.
- [5] P. Boolchand, X. Feng, W.J. Bresser, *J. NonCryst. Solids* 293 (2001) 248.
- [6] R. Rompicharla, D.I. Novita, P. Chen, P. Boolchand, M. Micoulaut, W. Huff, *J. Physics, Cond. Matt.* 20 (2008) 202101.
- [7] D.G. Georgiev, P. Boolchand, H. Eckert, M. Micoulaut, K. Jackson, *Europhys. Lett.* 62 (2003) 49.
- [8] M.F. Thorpe, P.M. Duxbury (Eds.), *Rigidity Theory and Applications*, Kluwer/Academic Press, 1999.
- [9] X.W. Feng, W.J. Bresser, P. Boolchand, *Phys. Rev. Lett.* 78 (1997) 4422.
- [10] M. Micoulaut, M. Popescu (Eds.), *Rigidity and Boolchand phases in nanomaterials*, INOE Publ. Bucarest, 2009.
- [11] G. Adam, J.H. Gibbs, *J. Chem. Phys.* 43 (1965) 139.
- [12] M. Micoulaut, *J. Phys. Cond. Matt.* 22 (2010) 285101.
- [13] G.G. Naumis, *Phys. Rev. E* 71 (2005) 026114.
- [14] F.J. Bermejo, C. Cabrillo, E. Bychkov, P. Fouquet, G. Ehlers, W. Häußler, D.L. Price, M.L. Saboungi, *Phys. Rev. Lett.* 100 (2009) 245902.
- [15] E.L. Gjersing, S. Sen, R.E. Youngman, *Phys. Rev. B* 82 (2010) 014203.
- [16] P.K. Gupta, J.C. Mauro, *J. Chem. Phys.* 130 (2009) 094503.
- [17] J.C. Mauro, P.K. Gupta, R.J. Loucks, *J. Chem. Phys.* 130 (2009) 234503.
- [18] M.M. Smedskjaer, J.C. Mauro, Y. Yue, *Phys. Rev. Lett.* 105 (2010) 115503.
- [19] M.M. Smedskjaer, J.C. Mauro, S. Sen, Y. Yue, *Chem. Mater.* 22 (2010) 5358.
- [20] M.M. Smedskjaer, J.C. Mauro, S. Sen, J. Deubener, Y. Yue, *J. Chem. Phys.* 133 (2010) 154509.
- [21] W.A. Kamitakahara, R.L. Cappelletti, P. Boolchand, B. Halfpap, F. Gompf, D.A. Neumann, H. Mutka, *Phys. Rev. B* 44 (1991) 94.
- [22] N.F. Mott, *Phil. Mag.* 19 (1969) 835.
- [23] Y. Vaills, T. Qu, M. Micoulaut, F. Chaimbault, P. Boolchand, *J. Phys. Cond. Matt.* 17 (2005) 4889.
- [24] P.H. Gaskell, M.C. Eckersley, A.C. Barnes, P. Chieux, *Nature* 350 (1991) 675.
- [25] X. Xue, J.F. Stebbins, *Phys. Chem. Miner.* 20 (1993) 297.
- [26] S.L. Tagg, R.E. Youngman, J.W. Zwanziger, *J. Phys. Chem.* 99 (1995) 5111.
- [27] M.C. Wilding, C.J. Benmore, J.A. Tangeman, S. Sampath, *Chem. Geol.* 213 (2004) 281.
- [28] T. Taniguchi, M. Okuno, T. Matsumoto, *J. NonCryst. Solids* 211 (1997) 56.
- [29] G.N. Greaves, *J. NonCryst. Solids* 71 (1985) 203.
- [30] J. Zhao, P.H. Gaskell, M.M. Cluckie, A.K. Soper, *J. NonCryst. Solids* 232–234 (1998) 721.
- [31] L. Cormier, D. Ghaleb, D.R. Neuville, J.M. Delaye, G. Calas, *J. NonCryst. Solids* 332 (2003) 255.
- [32] P. Righet, B.O. Mysen, *Silicate Glasses and Melts: Properties and Structure*, Elsevier, Amsterdam, 2005.
- [33] P.H. Poole, P.F. McMillan, G.H. Wolf, in: J.F. Stebbins, P.F. McMillan, D. Dingwell (Eds.), *Computer simulations of silicate melts*, *Rev. Mineralogy*, 32, 1995, p. 563.
- [34] G.S. Henderson, *Canad. Mineral.* 43 (2005) 1921.
- [35] S. Sen, G.N. Greaves, *Adv. Physics*. 56 (2007) 1.
- [36] A.N. Cormack, J. Du, T.R. Zeidler, *Phys. Chem. Chem. Phys.* 4 (2002) 3193.
- [37] X. Yuan, A.N. Cormack, *J. NonCrystalline Solids* 319 (2003) 31.
- [38] J. Du, A.N. Cormack, *J. NonCryst. Solids* 349 (2004) 66.
- [39] N. Bansal, R. Doremus, *Handbook of glass properties*, Academic Press, London, 1986.
- [40] A.C. Wright, A.G. Clare, B. Bachra, R.N. Sinclair, A.C. Hannon, B. Vessal, *Trans. Am. Ceram. Assoc.* 27 (1991) 239.
- [41] G.N. Greaves, A. Fontaine, P. Lagarde, D. Raoux, S.J. Gurman, *Nature* 293 (1981) 611.
- [42] G.S. Henderson, *J. NonCryst. Solids* 183 (1995) 43.
- [43] C. Mazzara, J. Jupille, A.-M. Flanck, P. Lagarde, *J. Phys. B* 104 (2000) 3438.
- [44] A.K. Pant, *Acta. Cryst.* B24 (1968) 1077.
- [45] T. Uchino, T. Yokoi, *J. Phys. Chem. B* 102 (1998) 8372.
- [46] J.L. Lagrange, *Mécanique Analytique*, Paris, 1788; J.C. Maxwell, *Philos. Mag.* 1864.
- [47] C. Bichara, J.-Y. Raty, J.-P. Gaspard, *Phys. Rev. B* 53 (1996) 206.
- [48] F. Inam, D.A. Drabold, M. Shatnawi, D. Tafen, P. Chen, S. Billinge, *J. Phys. Cond. Matt.* 19 (2007) 455206.
- [49] F. Inam, G. Chen, D.N. Tafen, D.A. Drabold, *Phys. Stat. Sol. B* 246 (2009) 1849.
- [50] M.F. Thorpe, D.J. Jacobs, M.V. Chubysnky, J.C. Phillips, *J. NonCryst. Solids* 266–269 (2000) 859.
- [51] M. Micoulaut, *Phys. Rev. B* 74 (2006) 184208.
- [52] M. Micoulaut, C. Otjacques, J.-Y. Raty, C. Bichara, *Phys. Rev. B* 81 (2010) 174206.
- [53] M. Bauchy, M. Micoulaut, M. Celino and C. Massobrio, *cond-mat/1007.10063*.
- [54] J. Du, R. Corrales, *Phys. Rev. B* 72 (2005) 092201.
- [55] X. Yuan, A.N. Cormack, *J. NonCryst. Solids* 319 (2003) 31.
- [56] M. Zhang, P. Boolchand, *Science* 266 (1994) 1355.
- [57] C.Y. Fang, H. Yinnon, D.R. Uhlmann, *J. NonCryst. Solids* 57 (1983) 465.
- [58] D.R. Uhlmann, *J. NonCryst. Solids* 7 (1972) 337.
- [59] M. Micoulaut, *Am. Mineral.* 93 (2008) 1732.
- [60] R. Azoulay, H. Thibierge, A. Brenac, *J. NonCryst. Solids* 18 (1975) 33.
- [61] P. Righet, *Geochim. Cosmochim. Acta* 48 (1984) 471.
- [62] P. Righet, M. Roskosz, J. Roux, *Chem. Geol.* 225 (2006) 388.
- [63] R.A. Narayanan, *Phys. Rev. B* 64 (2001) 134207.
- [64] P. Boolchand, D.G. Georgiev, B. Goodman, *J. Opt. Adv. Mater.* 3 (2001) 703.
- [65] M. Micoulaut, J.C. Phillips, *J. NonCryst. Solids* 353 (2007) 1732.
- [66] J. Horbach, W. Kob, K. Binder, *Chem. Geol.* 174 (2001) 87.
- [67] A. Meyer, D.B. Dingwell, H. Schober, *Europhys. Lett.* 59 (2002) 708.
- [68] J.O.M. Bockris, J.D. Mackenzie, J.A. Kitchener, *Trans. Faraday Soc.* 51 (1955) 1734.
- [69] K. Otto, M.E. Milberg, *J. Am. Ceram. Soc.* 51 (1968) 326.